JACS
JOURNAL OF THE AMERICAN CHEMICAL SOCIETY
Article
pubs.acs.org/JACS

De Novo Discovery of [Hdabco]BF_4 Molecular Ferroelectric Thin Film for Nonvolatile Low-Voltage Memories

Ping-Ping Shi, Yuan-Yuan Tang, Peng-Fei Li, Heng-Yun Ye,* and Ren-Gen Xiong*

Ordered Matter Science Research Center, Southeast University, Nanjing 211189, P. R. China

Supporting Information

ABSTRACT: To date, the field of ferroelectric random access memories (FeRAMs) is mainly dominated by inorganic ferroelectric thin films like Pb(Zr,Ti)O_3, which suffer from the issues of environmental harmfulness, high processing temperatures, and high fabrication costs. In these respects, molecular ferroelectric thin films are particularly advantageous and thus become promising alternatives to the conventional inorganic ones. For the prospect of FeRAMs applications, they should fulfill the requirements of effective polarization switching and low-voltage, high-speed operation. Despite recent advancements, molecular ferroelectric thin films with such high performance still remain a huge blank. Herein we present the first example of a large-area continuous biaxial molecular ferroelectric thin film that gets very close to the goal of application in FeRAMs: [Hdabco]BF_4 (dabco = diazabicyclo[2.2.2]octane). In addition to excellent film performance, it is the coexistence of a low coercive voltage of ∼12 V and ultrafast polarization switching at a significantly high frequency of 20 kHz that affords [Hdabco]BF_4 considerable potential for memory devices. Particularly, piezoresponse force microscopy (PFM) clearly demonstrates the four polarization directions and polarization switching at a low voltage down to ∼4.2 V (with an ∼150 nm thick film). This innovative work on high-performance molecular ferroelectric thin films, which can be compatible with wearable devices, will inject new vitality to the low-power information field.

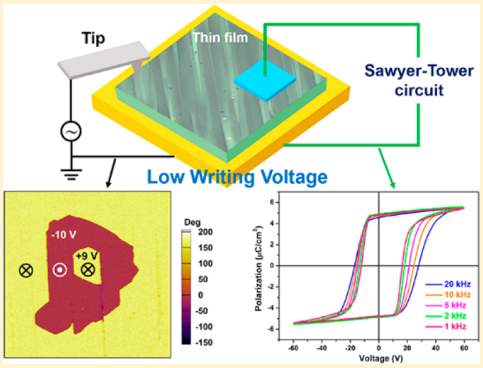

INTRODUCTION

The most intrinsic and widely used property of ferroelectrics is that the spontaneous polarization can be switched by applying an external electric field.[1] On the basis of polarization switching, data can be stored and read out, so that ferroelectrics become excellent candidates for ferroelectric random access memories (FeRAMs).[2] Currently, the ferroelectric thin films including Pb(Zr,Ti)O_3, $SrBi_2Ta_2O_9$, and $BiFeO_3$ are all known to be vital in commercial FeRAMs.[3] However, it is disadvantageous for the widespread application of FeRAMs that these inorganic thin films not only contain environmentally harmful heavy metals, but also require time-consuming, high-cost, and energy-intensive fabrication processes such as sputtering, pulsed laser deposition, etc.[4] Conversely, organic thin films can be deposited by using solution-based methods at room temperature in air, opening up the possibility of low-temperature, large-scale device fabrication for inexpensive high-performance electronics devices.[5] Hence, as a revolutionary innovation in the FeRAMs field, molecular ferroelectric thin films with advantages such as low cost, ease of processing, environmental friendliness, and biocompatibility are regarded as promising and viable alternatives or supplements to conventional inorganic ones.

In recent years, a number of molecular ferroelectrics with excellent ferroelectric properties have emerged.[6] However, there still exist several major challenges for their applications in FeRAMs: (i) the multiple polarization axes for effective polarization switching in the film form, (ii) the low-voltage operation, and (iii) the ultrafast polarization switching for high-speed operation. In contrast to inorganic ferroelectrics, the uniaxial nature always requires molecular ferroelectrics to be oriented in the desired polarization axis to achieve effective polarization switching, which is particularly difficult for the thin-film form.[7] That is why the remnant polarization of the uniaxial croconic acid film reported by Jiang et al. is 2 orders of magnitude lower than that of the single crystal.[6e,8] More importantly, even without the restriction on polarization axis, most of the known molecular ferroelectrics are still subject to the ferroelectric hysteresis loops available only at low frequencies and the relatively high coercive fields (E_c).[9] A recently discovered multiaxial molecular ferroelectric, quinuclidinium perrhenate, for instance, is unable to show ferroelectric behavior in the room-temperature phase due to the presence of a high E_c.[6f] For another notable example, 2-methylbenzimidazole (MBI), in addition to the difficulty of forming a large-area continuous thin film, the frequency enabling polarization switching is also not high enough to realize the large-scale applications.[10] All of these examples demonstrate how hard it is to meet the above conditions simultaneously in molecular ferroelectric thin films, let alone to facilitate FeRAMs.

Received: November 30, 2016
Published: January 6, 2017

DOI: 10.1021/jacs.6b12377
J. Am. Chem. Soc. 2017, 139, 1319−1324

In this way, [Hdabco]BF_4 (dabco = 1,4-diazabicyclo[2.2.2]-octane) (**1**) aroused our interest because of its biaxial characteristic. The ferroelectricity of a single crystal of **1** has been preliminarily disclosed by Katrusiak et al.;[11] however, the study on the thin film concerning practical applications was not included. Here, we present a large-area continuous thin film of **1** that combines a low coercive voltage of ~12 V and, equally important, ultrafast polarization switching at a considerably high frequency of 20 kHz. To the best of our knowledge, this is the first example of a molecular ferroelectric thin film which can couple so many superior properties and thus get so close to the practical level. Moreover, using piezoresponse force microscopy (PFM), we clearly demonstrated the relative polarization directions in the four kinds of domains, and offered direct experimental proof that the switching voltage can even be reduced to ~4.2 V with decreasing film thickness to ~150 nm. In combination with such a low operating voltage and good biocompatibility, this system is suitable for desirable wearable devices and bionics. Undoubtedly, this indicates the huge potential of molecular ferroelectric thin films and will greatly innovate and expand the field of FeRAMs.

RESULTS AND DISCUSSION

The ferroelectricity of the single-crystal samples of **1** has been confirmed by the measurements of *P*–*E* hysteresis loop and temperature-dependent dielectric constant.[11] The paraelectric-to-ferroelectric phase transition occurring at T_c (Curie temperature) = 374 K is accompanied by the symmetry change with 4/*mmmFmm*2 species. At room temperature, the ferroelectric phase adopts the orthorhombic space group $Pm2_1n$ (point group: *mm*2), whose polarization direction is confined to the [010]-direction by crystallographic symmetry. Considering its paraelectric phase with the tetragonal space group *P*4/*mmm* (point group: 4/*mmm*), the paraelectric-to-ferroelectric phase transition will give rise to spontaneous polarization in the [110]-direction, which coincides with the [010]-direction in the ferroelectric phase (Figure 1). Since there are four equivalent [110]-directions in the paraelectric phase, four equivalent polarization directions can consequently be found in the ferroelectric phase, as illustrated by the translucent red arrows in Figure 1. This indicates the biaxial feature of **1**, which is relatively rare in molecular ferroelectrics, and thus, two kinds of angles between domains can be theoretically predicted (i.e., 90° and 180°).

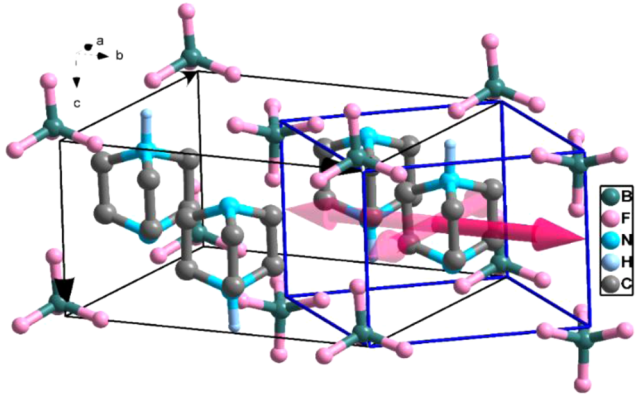

Figure 1. Relationship between the ferroelectric phase unit cell (black line) and the paraelectric phase unit cell (blue line) of **1**. Hydrogen atoms bonded to C atoms were omitted for clarity. The polarization direction (red arrow, [010]-direction) in the ferroelectric phase unit cell coincides with the [110]-direction of its paraelectric phase unit cell.

Distinct from the uniaxial ferroelectrics, multiaxial ones are particularly useful for forms of polycrystalline ceramics and thin films, in which the polarization can be switched more easily between multiple ferroelectric axes to achieve a larger value.[6f,7] No doubt, this very feature will be a deciding factor in the practical applications of molecular ferroelectrics. So, in order to further explore the application potential of **1** as a biaxial molecular ferroelectric, a simple and operative chemical solution routine was employed to fabricate the thin film. First, [Hdabco]BF_4 was dissolved into deionized water to form a homogeneous precursor aqueous solution. Then, a drop of precursor solution was carefully spread on a freshly cleaned ITO (indium tin oxide)-coated glass (conductive ITO was used as the bottom electrode). With controlled substrate temperature and edge-pinned crystallization, a uniform film consisting of continuous needle-like crystals with high coverage was obtained. By continuously rotating the film under orthogonally polarized light, the regular change of alternating bright and dark appearance induced by the crystal birefringence clearly indicates the good crystallinity and similar crystal orientation within the thin film of **1** (Figure 2a,b). As shown in Figure 2c, the high-quality film was also examined under atomic force microscopy (AFM).

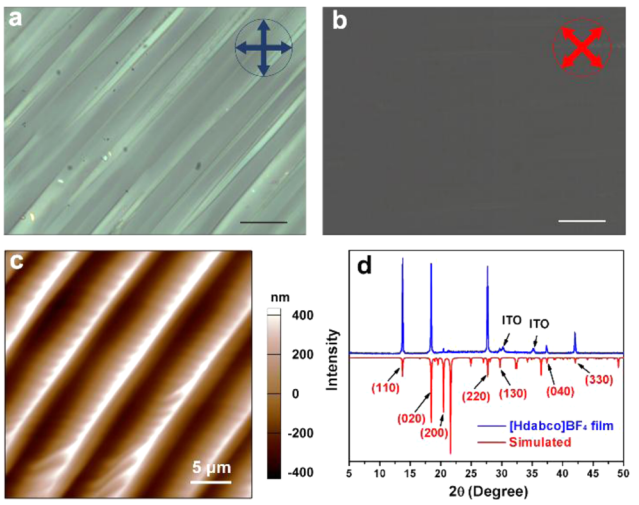

Figure 2. (a, b) Optical microscope (OM) photographs of a solid film of **1**, under orthogonally polarized light (scale bar: 20 μm). (c) The AFM image of the thin-film surface. (d) X-ray diffraction (XRD) pattern for the thin film of **1** deposited on ITO-glass and its comparison with that of the theoretically simulated counterpart.

Very interestingly, the inerratic allied needle-like microcrystals are periodically grown in situ on the ITO-coated substrate without any visible pinholes. The crystal domain growth tends to form an allied one-dimensional (1D) needle-like morphology during the drop fabrication method from solution. Such self-assembled ability can be attributed to the intrinsic parallel 1D hydrogen bonding effect along the [001]-direction as shown in Figure S1 (Supporting Information). The results of out-of-plane X-ray diffraction (XRD) measurement have also proved such a crystal domain arrangement. As shown in Figure 2d, the major out-of-plane diffractions of the thin film of **1** are (110), (020), (200), and (130), demonstrating that the

DOI: 10.1021/jacs.6b12377
J. Am. Chem. Soc. 2017, 139, 1319–1324

[001]-directional hydrogen bond chain lies in the plane of the substrate. The homogeneous light intensity under orthogonally polarized light indicates that this large-area thin film (mm^2 level) adopts the same crystal orientation (Figure S2, Supporting Information). Also, the average film thickness of 1.0 μm was revealed by a man-made gap on the film (Figure S3, Supporting Information).

On the basis of the high-quality thin film of **1** which has the preferred orientation, polarization switching was successfully achieved at room temperature by using macroscopic polarization versus external voltage hysteresis loop measurements. Specifically, a drop of liquid GaIn eutectic was used directionally as the top electrode, so the hysteresis loop measurements were conducted with the capacitor architecture of GaIn/[Hdabco]BF_4/ITO under the standard Sawyer–Tower circuit (Premier II Ferroeclectric Tester, Radiant Technologies). Rectangular P–E hysteresis loops are well-presented in Figure 3, affording indispensable proof of the

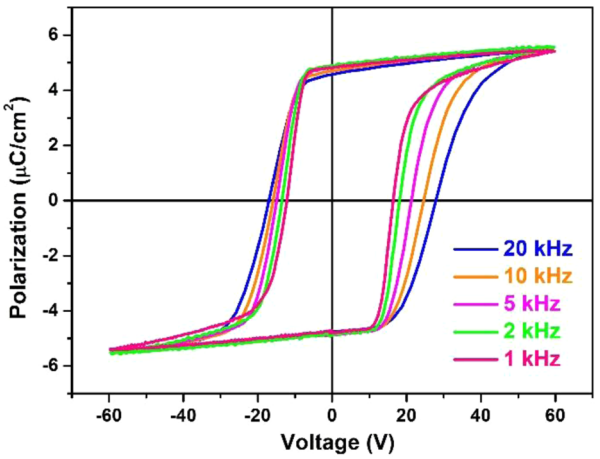

Figure 3. Room-temperature ferroelectric hysteresis loops of the thin film of **1** with ~1.0 μm thickness at different ac frequencies.

excellent ferroelectricity in **1** at room temperature. With the benefit from the desired capacitor thickness, the polarization can be switched under a moderate V_c (10–20 V) with different ac (alternating current) frequencies. Meanwhile, the thin film of **1** also displays a considerable P_r (remnant polarization) value of 4.9 $\mu C/cm^2$ even with a great increase of the driving frequency, which approaches the reported value of the single-crystal sample and exceeds those of MBI and [Hdabco]ClO_4 thin films. In addition, asymmetry with a slightly positive shift of E_c was also observed on this asymmetric GaIn/[Hdabco]BF_4/ITO capacitor, which can be reduced by decreasing the driving ac frequency. As depicted in Figure 3, with a fixed external electric voltage amplitude (60 V), the asymmetry can be greatly restored from 20 to 1 kHz. Also, with the decrease of the driving ac frequency from 20 kHz to 1 kHz, E_c decreases from 230 to 140 kV/cm, the reason for which is discussed in the Supporting Information. When the liquid electrode of GaIn eutectic was replaced with sputtered Au, the perfect ferroelectric hysteresis loops can also be obtained (the results are shown in Figure S4, Supporting Information). Above all, the most important and attractive characteristic of the thin film of **1** is the surprisingly ultrafast polarization switching that can be attained even at the really high frequency of 20 kHz. To our knowledge, it was first observed in molecular ferroelectric thin films, which will play a valuable role in the development of high-speed FeRAM devices.

For the sake of further investigating the microscopic ferroelectric polarization, we carried out density functional calculations based on the Berry phase method developed by Kingsmith and Vanderbilt.[12] The first-principles calculations were performed within the framework of density functional theory (DFT) implemented in the Vienna ab initio Simulation Package (VASP).[13] The energy cutoff for the expansion of the wave functions was fixed at 500 eV, and the exchange–correlation interactions were treated within the generalized gradient approximation of the Perdew–Burke–Ernzerhof type.[14] For the integrations over the k-space, we applied a 3 × 3 × 5 k-point mesh. The crystal structure at 156 K[15] was used as the original model for evaluating the ferroelectric polarization. In the model, atoms were allowed to relax until the atomic forces on each atom are smaller than 0.01 eV/Å, on which basis the evolution of spontaneous polarization from the centrosymmetric structure (λ = 0) to the optimized polar structure (λ = 1) was calculated (Figure 4). The theoretically

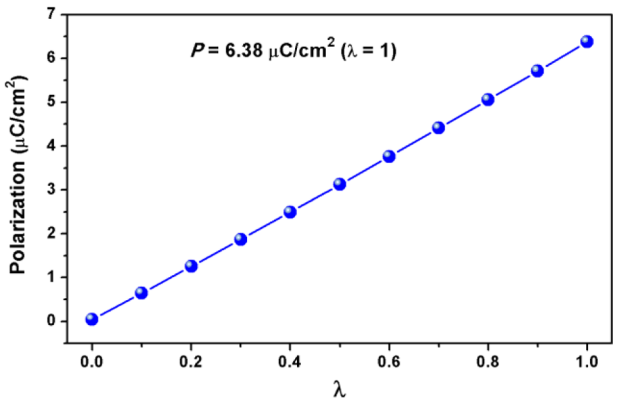

Figure 4. Polarization of **1** as a function of λ evaluated by Berry phase calculation.

predicted polarization of about 6.38 $\mu C/cm^2$ is slightly larger than the value (5.11 $\mu C/cm^2$) obtained by the point charge model analysis (Table S1, Supporting Information), and is close to the experimental P_r value.

Ferroelectric properties are well-known to depend significantly on the microscopic domain structure and domain dynamics, which are thus essential for the practical applications. In this respect, piezoresponse force microscopy (PFM) has emerged as a powerful tool for the characterizations of ferroelectric materials at the nanometer scale, by providing nondestructive visualization of the statics and dynamics of ferroelectric domains with unprecedented spatial resolution.[16] Each PFM image can be characterized by the amplitude and phase parameters that concern the value of the piezoelectric coefficient and the orientation of the domain polarization, respectively. The as-grown domain structure of the thin film of **1** is mainly dominated by the large-area single-domain state, as displayed by the uniform phase signal achieved from the three random regions (Figure S5, Supporting Information). When the sample temperature is increased to above T_c and then decreased to room temperature, the domain structure in the annealed state is strikingly different from that in the as-grown state. Figure S6 (Supporting Information) presents the images constructed by vertical PFM amplitude and phase in the

DOI: 10.1021/jacs.6b12377
J. Am. Chem. Soc. 2017, 139, 1319–1324

annealed state, which reveal the typical stripe domain structure and superimposed irregular domain pattern.

For a depiction of the distinct polarization directions of the four types of domains in the annealed state, the vertical and lateral PFM (VPFM and LPFM) images have been acquired and analyzed in a smaller area of 2 μm × 2 μm. As shown in Figure 5, notably, the striking 180° phase contrasts in the phase

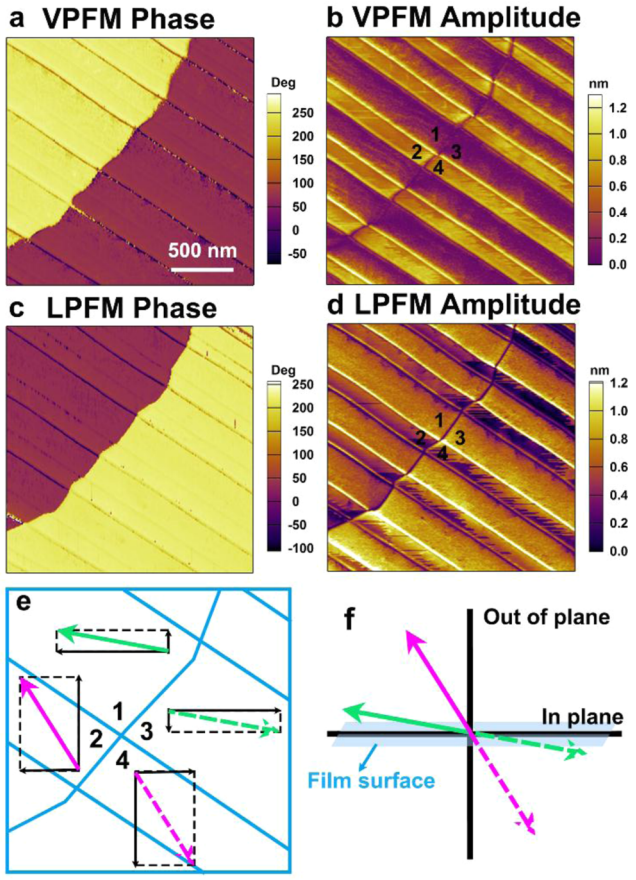

Figure 5. (a–d) VPFM and LPFM phase and amplitude images in the thin film of **1**. (e) A schematic geometry of polarization directions in the four kinds of domains at the plane constructed by the vertical and horizontal directions of the film surface, deduced from the amplitude signals and phase contrasts in two PFM modes. (f) The four polarization directions of the film relative to the film surface.

images and the nearly equal amplitude signals in the amplitude images can be found on the two sides of the irregular domain wall, indicating a 180° domain wall. Meanwhile, with respect to the two kinds of stripe domains, both the same phase contrasts and the different amplitude signals observed in the two PFM modes are indicative of their different and nonantiparallel polarization directions. Hence, the domain walls separated by the stripe domains should be defined as the non-180° ones, like that found in $BiFeO_3$ (BFO).[17] These results unambiguously confirm the coexistence of 180° and non-180° domain walls in the thin film of **1**.

More importantly, in view of the amplitude signals and phase contrasts in the two PFM modes, we can roughly estimate the polarization directions in the four kinds of domains at the plane constructed by the vertical and horizontal directions of the film surface. To be specific, the phase contrasts in two different components decide the corresponding directions, while one contrast is randomly designated as a certain direction and another contrast as its antiparallel direction (Figure 5e). Then, the magnitude of the vector is determined by averaging the PFM amplitude value. With a combination of the polarization vectors in the vertical and lateral directions, the polarization directions of domains at this plane can consequently be estimated. As shown in Figure 5f, the 180° and non-180°(which deviates slightly from 90°, since these polarization directions are only composed by two components) angles between the polarization directions agree with the above estimation of polarization directions by the crystal structures in two phases and manifest the existence of two polar axes. Moreover, it can be seen that the polarization directions in two domains have a relatively large component perpendicular to the substrate, while another two have a small component. Due to the multiaxial characteristic, the direction with the small component can be switched to the one with a large component, thus guaranteeing the high performance in the thin-film form. This phenomenon can somewhat explain the high P_r value of the thin film of **1**, which is close to that of the single-crystal sample.

In addition to the above-mentioned P–E hysteresis loops, the evolution of domain structure during polarization switching is also a chief subject for characterizing ferroelectric thin films. Hence, we carried out local polarization manipulation experiments in the thin films of **1** with different thicknesses. Figure 6a–c shows the VPFM phase images of 2, 1, and 0.6 μm thick films after writing box-in-box patterns with reversed dc bias in the center. Clear and successive reversals of phase contrasts

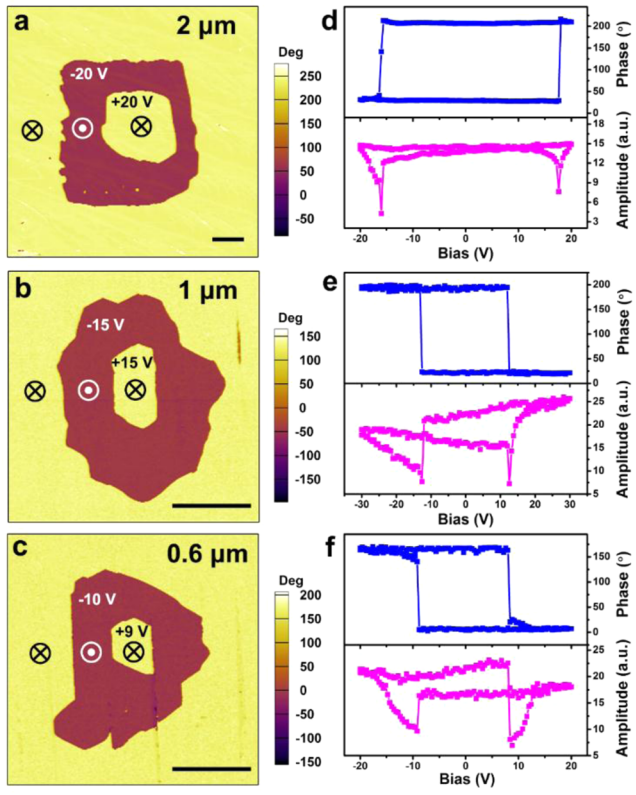

Figure 6. Ferroelectric polarization switching by PFM for the thin films of **1** with different thicknesses. (a–c) The VPFM phase images for 2 μm (a), 1 μm (b), and 0.6 μm (c) thick films with written box-in-box patterns under reversed dc bias. Scale bar, 5 μm. (d–f) The VPFM phase and amplitude hysteresis loops measured during the switching processes for 2 μm (d), 1 μm (e), and 0.6 μm (f) thick films.

DOI: 10.1021/jacs.6b12377
J. Am. Chem. Soc. 2017, 139, 1319–1324

(~180°) appear, indicating that the polarizations in these thin films can be switched forth and back. In Figure S7 (Supporting Information) and its caption, we take a 0.6 μm thick film as an example to detail the entire switching process, which offers the direct observation of domain switching at the low writing voltage down to 10 V. The switched domains can remain perfectly stable for more than 10 h (Figure S7d), and thus, the possible contribution of PFM signal from the electrochemical phenomena is excluded.[18] Furthermore, during the switching of ferroelectric domains, there are no obvious traces of deformation in the corresponding surface morphologies. All of these observations provide direct evidence that the domains in the thin film of **1** are switchable under a low external field, being characteristic of a ferroelectric material. It is based on the polarization switching of ferroelectric domains that information can be written in the thin film of **1** and affords it potential FeRAMs applications.

Local PFM spectroscopic experiments have also been performed to further verify the ferroelectric characteristics of the thin film of **1**. Under the resonance-enhanced PFM mode, the characteristic hysteresis and butterfly loops typical for the switching of ferroelectric domains were clearly observed by applying an ac electric field superimposed on a dc triangular square-stepping wave (Figure 6d–f). By averaging the minima of the amplitude hysteresis loops, we can estimate that the local coercive voltage (V_c) values for 2, 1, and 0.6 μm thick films are 16.8, 12.7, and 8.5 V, respectively. It is obvious that the V_c depends strongly on the sample thickness. Therefore, we tried to fabricate a 150 nm thick film, and found that the V_c can be reduced down to 4.2 V (Figure S8, Supporting Information). The dependence of V_c on film thickness (d) is depicted in Figure S9 (Supporting Information), which is in good agreement with the semiempirical scaling law derived by Kay and Dunn, i.e., $V_c = bd^{1/3}$.[1c,19] Such a low operating voltage, together with the high P_r and the ultrafast polarization switching, will be very desirable for FeRAM devices.

CONCLUSION

The large-area continuous thin film of **1**, which displays good crystallinity and preferable crystal orientation, was fabricated by a simple and effective solution method. The 1D needle-like morphology of the thin film is attributed to the intrinsic parallel 1D hydrogen bonding effect along the [001]-direction. Benefiting from the presence of two ferroelectric axes and preferable crystal orientation, the molecular ferroelectric thin film of **1** maintains a high P_r of 4.9 μC/cm^2. This value is close to those of the single-crystal sample and the calculated values based on the Berry phase calculation and the point charge model analysis. In addition, from the P–E hysteresis loops measured on the thin-film samples, the most wonderful results concern the extremely low V_c of about 10 V and the ultrafast polarization switching at a relatively high frequency of 20 kHz. By using the PFM technique, it is the coexistence of 180° and non-180° domain walls, the presence of two polar axes, and the switchable ferroelectric domains under an external voltage as low as 4.2 V that are also fully demonstrated. In summary, this example of molecular ferroelectric thin film with so many merits is presented for the first time. It satisfies the essential criteria of practical FeRAMs, and will inject new vitality to the field of molecular ferroelectric thin films.

EXPERIMENTAL SECTION

Materials. All reagents and solvents in the syntheses were of reagent grade and used without further purification. **1** was prepared by slow evaporation of the ethanol solution of dabco and HBF_4 in a 1:1 molar ratio.

Thin-Film Fabrication and *P*–*E* Measurements. Ferroelectric thin films of **1** were grown by means of the conventional drop-casting and spin-coating methods. The detailed process is described as follows. First, commercial quadrate ITO (indium tin oxide)-coated glass substrate (a = 15 mm) was ultrasonically cleaned sequentially with toluene, acetone, ethanol, and deionized water for 20 min at a time. Next, the substrate was treated under UV-Oz1 atm (65 °C, 30 min) for the generation of a hydrophilic surface. After that, a simple chemical solution process was employed to fabricate the film. The powder sample of **1** was dissolved in deionized water to form a homogeneous precursor solution. Then, a drop of solution was carefully spread on the freshly cleaned ITO-coated glass (conductive ITO was used as the bottom electrode). With controlled substrate temperature (50 ± 1 °C) and edge-pinned-crystallization, large-area dendritic crystals were in situ grown on the ITO-coated glass with a perfectly uniform coverage rate. The film thickness was measured with a man-made gap using AFM. For the films with different thicknesses, precursor solutions with different concentrations (100, 50, and 10 mg/mL) were applied for the drop-casting process. The specific relationship between the film thickness and the concentration of aqueous solution for the drop-casting method is presented in Figure S10 (Supporting Information). After that, the top electrodes were directly selected as liquid GaIn eutectic or fabricated through sputtering gold target with a metal shadow mask (Φ = 0.2–1 mm). Gold sputtering was conducted within 10 cycles with a period time of 60 s. Next, the P–E measurements were performed on a probe station equipped with a Precision Premier II Ferroelectric Tester (Radiant Technologies), and typical ac voltage with a triangular wave was applied at different frequencies.

For the 150 nm film, a typical spin-coating process (6000 rpm, 60 s) was employed with the precursor methanol solution containing [Hdabco]BF_4 (10 mg/mL). During the spin-coating, microcrystals were grown in situ on the ITO-coated glass. A low-temperature annealing process (35 °C, 30 min) was carried out to remove any residual solvents. The uniformity and continuity are worse for these samples than for the drop-casting film based on aqueous solution (Figure S11, Supporting Information).

PFM Measurements. Thin films were used for the PFM measurements. Nanoscale polarization imaging and local switching spectroscopy were carried out using a resonant-enhanced piezoresponse force microscopy (MFP-3D, Asylum Research). Conductive Pt/Ir-coated silicon probes (EFM-50, Nanoworld) were used for domain imaging and polarization switching studies. Resonant-enhanced PFM mode was applied to enhance the signal, with a typical ac voltage of 2.0 V at ~360 kHz.

ASSOCIATED CONTENT

Supporting Information

The Supporting Information is available free of charge on the ACS Publications website at DOI: 10.1021/jacs.6b12377.

Figures S1–S11, Table S1, and discussion (PDF)

AUTHOR INFORMATION

Corresponding Authors

*hyye@seu.edu.cn

*xiongrg@seu.edu.cn

ORCID

Ren-Gen Xiong: 0000-0003-2364-0193

Notes

The authors declare no competing financial interest.

DOI: 10.1021/jacs.6b12377
J. Am. Chem. Soc. 2017, 139, 1319–1324

■ ACKNOWLEDGMENTS

This work was supported by 973 project (2014CB932103) and the National Natural Science Foundation of China (21290172, 91422301, 21427801, and 21573041).

■ REFERENCES

(1) (a) Lines, M. E.; Glass, A. M. *Principles and Applications of Ferroelectrics and Related Materials*; Clarendon Press: Oxford, UK, 1977. (b) Ye, Z.-G. *Handbook of Advanced Dielectric, Piezoelectric and Ferroelectric Materials: Synthesis, Properties and Applications*; Elsevier, 2008. (c) Scott, J. *Science* **2007**, *315*, 954. (d) Shi, P.-P.; Tang, Y.-Y.; Li, P.-F.; Liao, W.-Q.; Wang, Z.-X.; Ye, Q.; Xiong, R.-G. *Chem. Soc. Rev.* **2016**, *45*, 3811.

(2) Ishiwara, H. J. *J. Nanosci. Nanotechnol.* **2012**, *12*, 7619.

(3) Park, B.; Kang, B.; Bu, S.; Noh, T.; Lee, J.; Jo, W. *Nature* **1999**, *401*, 682.

(4) Haertling, G. H. *J. Am. Ceram. Soc.* **1999**, *82*, 797.

(5) Rigas, G. P.; Payne, M. M.; Anthony, J. E.; Horton, P. N.; Castro, F. A.; Shkunov, M. *Nat. Commun.* **2016**, *7*, 13531.

(6) (a) Tayi, A. S.; Shveyd, A. K.; Sue, A. C.; Szarko, J. M.; Rolczynski, B. S.; Cao, D.; Kennedy, T. J.; Sarjeant, A. A.; Stern, C. L.; Paxton, W. F.; Wu, W.; Dey, S. K.; Fahrenbach, A. C.; Guest, J. R.; Mohseni, H.; Chen, L. X.; Wang, K. L.; Stoddart, J. F.; Stupp, S. I. *Nature* **2012**, *488*, 485. (b) Tayi, A. S.; Kaeser, A.; Matsumoto, M.; Aida, T.; Stupp, S. I. *Nat. Chem.* **2015**, *7*, 281. (c) Owczarek, M.; Hujsak, K. A.; Ferris, D. P.; Prokofjevs, A.; Majerz, I.; Szklarz, P.; Zhang, H.; Sarjeant, A. A.; Stern, C. L.; Jakubas, R.; Hong, S.; Dravid, V. P.; Stoddart, J. F. *Nat. Commun.* **2016**, *7*, 13108. (d) Fu, D. W.; Cai, H. L.; Liu, Y.; Ye, Q.; Zhang, W.; Zhang, Y.; Chen, X. Y.; Giovannetti, G.; Capone, M.; Li, J.; Xiong, R. G. *Science* **2013**, *339*, 425. (e) Horiuchi, S.; Tokunaga, Y.; Giovannetti, G.; Picozzi, S.; Itoh, H.; Shimano, R.; Kumai, R.; Tokura, Y. *Nature* **2010**, *463*, 789. (f) Harada, J.; Shimojo, T.; Oyamaguchi, H.; Hasegawa, H.; Takahashi, Y.; Satomi, K.; Suzuki, Y.; Kawamata, J.; Inabe, T. *Nat. Chem.* **2016**, *8*, 946. (g) Tang, Y.-Y.; Zhang, W.-Y.; Li, P.-F.; Ye, H.-Y.; You, Y.-M.; Xiong, R.-G. *J. Am. Chem. Soc.* **2016**, *138*, 15784. (h) Sato, O. *Nat. Chem.* **2016**, *8*, 644. (i) Yao, Z. S.; Yamamoto, K.; Cai, H. L.; Takahashi, K.; Sato, O. *J. Am. Chem. Soc.* **2016**, *138*, 12005. (j) Chen, S.; Zeng, X. C. J. *J. Am. Chem. Soc.* **2014**, *136*, 6428.

(7) Ye, H.-Y.; Ge, J.-Z.; Tang, Y.-Y.; Li, P.-F.; Zhang, Y.; You, Y.-M.; Xiong, R.-G. *J. Am. Chem. Soc.* **2016**, *138*, 13175.

(8) Jiang, X.; Lu, H.; Yin, Y.; Zhang, X.; Wang, X.; Yu, L.; Ahmadi, Z.; Costa, P. S.; DiChiara, A. D.; Cheng, X.; Gruverman, A.; Enders, A.; Xu, X. *Appl. Phys. Lett.* **2016**, *109*, 102902.

(9) (a) Zhang, W.; Chen, L. Z.; Xiong, R. G.; Nakamura, T.; Huang, S. D. *J. Am. Chem. Soc.* **2009**, *131*, 12544. (b) Szafrański, M.; Katrusiak, A. *Phys. Rev. B: Condens. Matter Mater. Phys.* **2006**, *73*, 134111. (c) Szafrański, M. *Phys. Rev. B: Condens. Matter Mater. Phys.* **2005**, *72*, 054122. (d) Horiuchi, S.; Ishii, F.; Kumai, R.; Okimoto, Y.; Tachibana, H.; Nagaosa, N.; Tokura, Y. *Nat. Mater.* **2005**, *4*, 163. (e) Akutagawa, T.; Koshinaka, H.; Sato, D.; Takeda, S.; Noro, S.; Takahashi, H.; Kumai, R.; Tokura, Y.; Nakamura, T. *Nat. Mater.* **2009**, *8*, 342. (f) Zhang, Y.; Liao, W. Q.; Fu, D. W.; Ye, H. Y.; Chen, Z. N.; Xiong, R. G. *J. Am. Chem. Soc.* **2015**, *137*, 4928.

(10) Noda, Y.; Yamada, T.; Kobayashi, K.; Kumai, R.; Horiuchi, S.; Kagawa, F.; Hasegawa, T. *Adv. Mater.* **2015**, *27*, 6475.

(11) Katrusiak, A.; Szafrański, M. *Phys. Rev. Lett.* **1999**, *82*, 576.

(12) (a) Kingsmith, R. D.; Vanderbilt, D. *Phys. Rev. B: Condens. Matter Mater. Phys.* **1993**, *47*, 1651. (b) Vanderbilt, D.; Kingsmith, R. D. *Phys. Rev. B: Condens. Matter Mater. Phys.* **1993**, *48*, 4442.

(13) (a) Kresse, G.; Furthmuller, J. *Phys. Rev. B: Condens. Matter Mater. Phys.* **1996**, *54*, 11169. (b) Kresse, G.; Furthmuller, J. *Comput. Mater. Sci.* **1996**, *6*, 15.

(14) Perdew, J. P.; Burke, K.; Ernzerhof, M. *Phys. Rev. Lett.* **1996**, *77*, 3865.

(15) Budzianowski, A.; Katrusiak, A.; Szafranski, M. J. *J. Phys. Chem. B* **2008**, *112*, 16619.

(16) (a) Balke, N.; Winchester, B.; Ren, W.; Chu, Y. H.; Morozovska, A. N.; Eliseev, E. A.; Huijben, M.; Vasudevan, R. K.; Maksymovych, P.; Britson, J.; Jesse, S.; Kornev, I.; Ramesh, R.; Bellaiche, L.; Chen, L. Q.; Kalinin, S. V. *Nat. Phys.* **2011**, *8*, 81. (b) Garcia, V.; Fusil, S.; Bouzehouane, K.; Enouz-Vedrenne, S.; Mathur, N. D.; Barthelemy, A.; Bibes, M. *Nature* **2009**, *460*, 81. (c) Lee, D.; Lu, H.; Gu, Y.; Choi, S.-Y.; Li, S.-D.; Ryu, S.; Paudel, T. R.; Song, K.; Mikheev, E.; Lee, S.; Stemmer, S.; Tenne, D. A.; Oh, S. H.; Tsymbal, E. Y.; Wu, X.; Chen, L.-Q.; Gruverman, A.; Eom, C. B. *Science* **2015**, *349*, 1314.

(17) (a) Martin, L. W.; Rappe, A. M. *Nat. Rev. Mater.* **2016**, *2*, 16087. (b) Yang, S. Y.; Seidel, J.; Byrnes, S. J.; Shafer, P.; Yang, C. H.; Rossell, M. D.; Yu, P.; Chu, Y. H.; Scott, J. F.; Ager, J. W., 3rd; Martin, L. W.; Ramesh, R. *Nat. Nanotechnol.* **2010**, *5*, 143.

(18) Kalinin, S. V.; Jesse, S.; Tselev, A.; Baddorf, A. P.; Balke, N. *ACS Nano* **2011**, *5*, 5683.

(19) (a) Kay, H.; Dunn, J. *Philos. Mag.* **1962**, *7*, 2027. (b) Dawber, M.; Rabe, K.; Scott, J. *Rev. Mod. Phys.* **2005**, *77*, 1083.

DOI: 10.1021/jacs.6b12377
J. Am. Chem. Soc. 2017, 139, 1319−1324